

Stable hZW10 kinetochore residency, mediated by hZwint-1 interaction, is essential for the mitotic checkpoint

Jakub K. Famulski,¹ Larissa Vos,¹ Xuejun Sun,² and Gordon Chan^{1,2}

¹Department of Oncology, University of Alberta, Edmonton, Alberta, Canada T6G 1Z2

²Experimental Oncology, Cross Cancer Institute, Edmonton, Alberta, Canada T6G 1Z2

The mitotic checkpoint is an essential surveillance mechanism that ensures high fidelity chromosome segregation during mitosis. Mitotic checkpoint function depends on numerous kinetochore proteins, including ZW10, ROD, and Zwilch (the ROD-ZW10-Zwilch complex). Through an extensive mutagenesis screen of hZW10, we have mapped the kinetochore localization domain of hZW10 as well as the hZwint-1 interaction domain. We find that hZwint-1–noninteracting mutants still localize

to kinetochores. In addition, using fluorescence recovery after photobleaching, we have found that hZW10 residency at metaphase kinetochores is brief (half-time of 13 s). However, during prometaphase or at unattached kinetochores, enhanced green fluorescent protein–hZW10 becomes a stable component of the kinetochore. Moreover, we find that stable hZW10 kinetochore residency at pro-metaphase kinetochores is dependent on its interaction with hZwint-1, and is essential for mitotic checkpoint arrest.

Introduction

High fidelity chromosome segregation is essential for the maintenance of genomic stability. The mitotic checkpoint is a fail-safe mechanism that prevents premature anaphase onset and ensures accurate chromosome segregation. The mitotic checkpoint functions by monitoring proper kinetochore–microtubule (MT) attachments as well as chromosome alignment at the metaphase plate (Rieder et al., 1994; Skibbens et al., 1995). It is composed of several evolutionarily conserved kinetochore proteins including the MADs, the BUBs, and Mps1, as well as ZW10, ROD, and Zwilch (for reviews see Chan et al., 2005; Karess, 2005). These proteins monitor kinetochore-MT attachment and chromosome alignment and participate in the generation and amplification of the “wait anaphase” signal. BubR1, Bub3, Mad2, and Cdc20 are known to function as a mitotic checkpoint complex that directly inhibits the anaphase-promoting complex/cyclosome, an E3 ubiquitin ligase complex that drives ubiquitin-mediated degradation of key mitotic substrates that are required for the maintenance of metaphase arrest (Sudakin et al., 2001). Through the mitotic checkpoint complex, the mitotic checkpoint can initiate and maintain mitotic

arrest even in the presence of a single unattached kinetochore (Rieder et al., 1994).

ZW10 and ROD are recently recognized essential components of the mitotic checkpoint (Chan et al., 2000; Kops et al., 2005; for review see Karess, 2005). Identified in *Drosophila melanogaster*, ZW10 and ROD mutants exhibit identical mitotic phenotypes, including high rates of aneuploidy and chromosome missegregation stemming from the lack of mitotic checkpoint function (Karess and Glover, 1989; Williams et al., 1992; Scaerou et al., 1999; Basto et al., 2000). hZW10 has been shown to be required for hMad1 and hMad2 kinetochore recruitment, which may explain the ZW10 mutant phenotypes (Buffin et al., 2005; Kops et al., 2005). However, the exact molecular functions of hZW10 or hROD within the mitotic checkpoint remain unknown. ROD and ZW10 are evolutionarily conserved from *Caenorhabditis elegans* to humans yet lack homologues in yeast (Starr et al., 1997). This suggests that ZW10 and ROD may represent an arm of the mitotic checkpoint that evolved to maintain genomic stability of the larger and more complex higher eukaryote genomes. During mitosis, ZW10 and ROD interact with another mitotic checkpoint protein, Zwilch, and form an evolutionarily conserved complex (ROD-ZW10-Zwilch [RZZ]) that localizes to kinetochores from early prometaphase until the onset of anaphase (Williams and Goldberg, 1994; Williams et al., 1996, 2003). The RZZ complex is known to be required for kinetochore

Correspondence to Gordon Chan: gordonch@cancerboard.ab.ca

Abbreviations used in this paper: ACA, anticentromere antibody; MT, microtubule; PEI, polyethyleneimine; RZZ, ROD-ZW10-Zwilch.

The online version of this paper contains supplemental material.

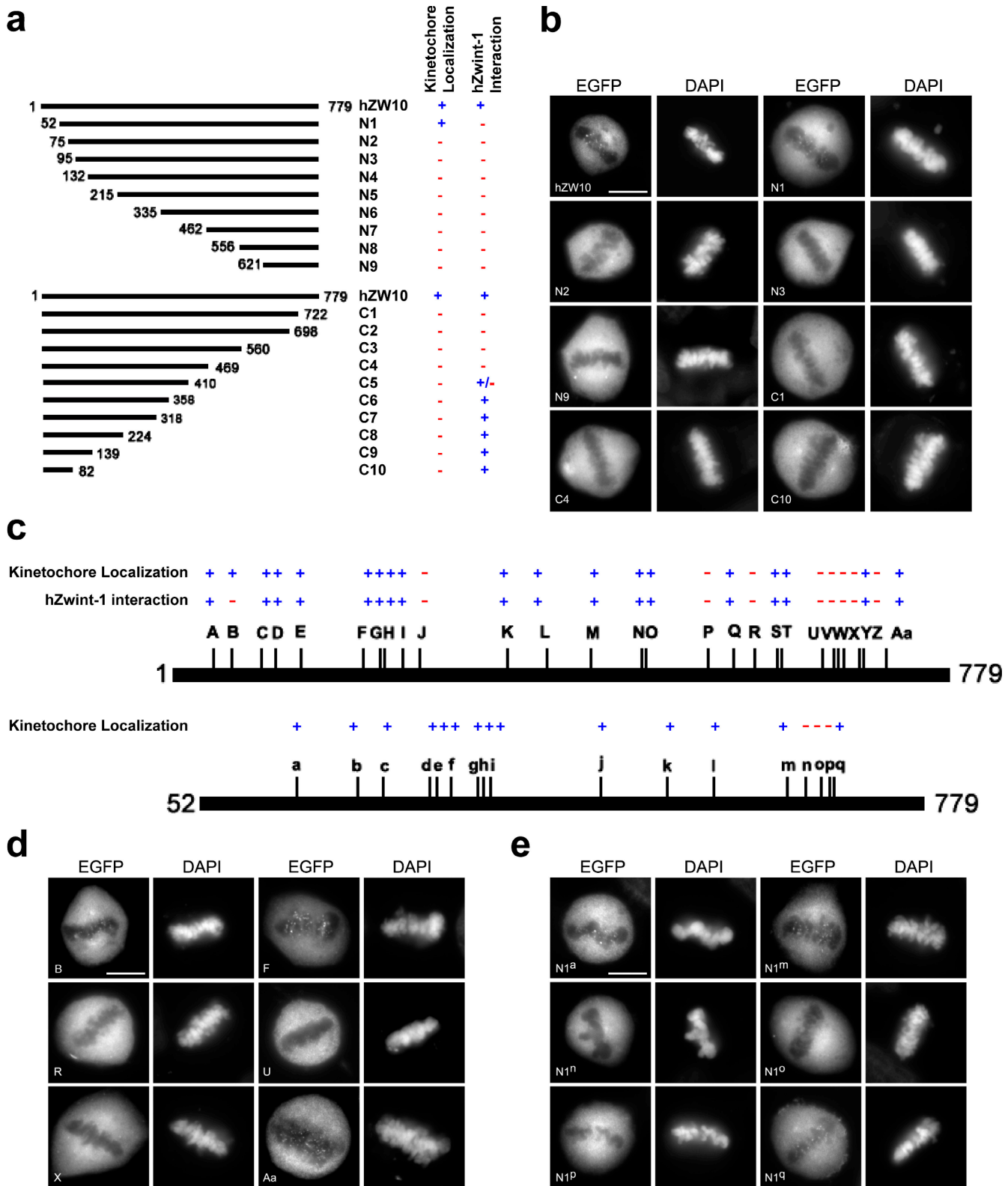


Figure 1. An extensive mutagenesis screen for the hZW10 kinetochore localization and hZwint-1 interaction domains. (a) A schematic diagram depicting N- and C-terminal hZW10 deletion constructs. Amino acid sizes are indicated. Yeast two-hybrid interaction with hZwint-1 and kinetochore localization are indicated by a blue plus sign for positive results and a red minus sign for negative results. (b) HeLa cells transiently transfected with EGFP-hZW10 N- and C-terminal deletion constructs were analyzed for kinetochore localization during mitosis with fluorescence microscopy. Representative images show that only N-terminal deletion N1 retained the ability to localize to the kinetochore. All mutants behaved similarly at both prometaphase and metaphase kinetochores. Bar, 10 μ m. (c) A schematic diagram depicting the locations of the pentapeptide insertion mutants generated in the hZW10 cDNA (aa 1–779) and the hZW10^{N1} cDNA (aa 52–779). Yeast two-hybrid interaction with hZwint-1 and kinetochore localization are indicated by a blue plus sign for positive interaction and a red minus sign for negative interaction. (d) HeLa cells transiently transfected with the EGFP-hZW10 insertion mutant constructs were analyzed

recruitment of the MT motor dynein/dynactin (Starr et al., 1998). Dynein/dynactin was found to directly interact with the RZZ complex in a yeast two-hybrid screen, which identified dynamin, a dynactin subunit, as an interactor of hZW10 (Starr et al., 1998; Yang et al., 2007). Kinetochore dynein/dynactin is, in turn, required for chromosomal congression, resulting in chromosome alignment at the metaphase plate as well as transport of mitotic checkpoint proteins off kinetochores (Howell et al., 2001; Yang et al., 2007). Before the onset of anaphase, *D. melanogaster* ROD has been observed to travel from kinetochores along kinetochore-MTs toward the spindle poles but only once chromosomes became bioriented (Scaerou et al., 1999; Basto et al., 2004). This movement of dmROD along kinetochore-MTs is also dependent on kinetochore dynein/dynactin. Dynein/dynactin-mediated transport of ROD, ZW10, and other mitotic checkpoint proteins off kinetochores in response to biorientation of chromosomes has been hypothesized to contribute to the silencing of the mitotic checkpoint (Howell et al., 2001; Wojcik et al., 2001).

Localization of hROD and hZW10 to kinetochores is correlated with mitotic checkpoint function, as implicated by anti-hZW10 and anti-hROD antibody microinjection experiments (Chan et al., 2000). Understanding how ROD and ZW10 localize to and behave at kinetochores is thus essential for determining the mitotic checkpoint functions of the RZZ complex. hZW10 kinetochore localization has been attributed to the interaction between hZW10 and hZwint-1. hZwint-1 was identified in a yeast two-hybrid screen for hZW10-interacting proteins and is thought to function as a scaffold for hZW10 at kinetochores (Starr et al., 2000). siRNA knockdown of hZwint-1 has been shown to result in the loss of kinetochore hZW10, thus suggesting that hZwint-1 is required for hZW10 recruitment to kinetochores during mitosis (H. Wang et al., 2004). However, experiments mapping the hZwint-1 interaction domain of hZW10 have thus far been contradictory. Starr et al. (2000) had originally mapped the hZwint-1 interaction domain to the C terminus of hZW10 yet, in a more recent paper, H. Wang et al. (2004) showed that the N terminus of hZW10 is sufficient for hZwint-1 interaction as well as kinetochore localization. To clarify the location of the hZwint-1 interaction, as well as that of the kinetochore localization domains of hZW10, we undertook a very detailed structure function study of hZW10. We have found that the N terminus of hZW10 is indeed sufficient for hZwint-1 interaction; however, it is not sufficient for kinetochore localization. Through our mutagenesis approach we have also discovered that hZW10 kinetochore localization may not solely depend on its interaction with hZwint-1. Instead, we find that the interaction between hZwint-1 and hZW10 increases hZW10 residency at kinetochores lacking proper kinetochore-MT attachments and that this increased residency is essential for proper function of the mitotic checkpoint.

Results

hZW10 kinetochore localization requires both the C and N terminus

Previous studies have indicated that the kinetochore localization domain of hZW10 mapped to its far N terminus (aa 1–80; H. Wang et al., 2004). In addition, this N-terminal domain was shown by the yeast two-hybrid assay to be sufficient for hZwint-1 interaction, thus linking hZwint-1 interaction with hZW10 kinetochore localization. However, Starr et al. (2000), also using the yeast two-hybrid assay, originally showed that the C terminus of hZW10 was required for the hZwint-1 interaction and therefore, presumably, hZW10 kinetochore localization. Thus, it appears that the locations of the hZwint-1 interaction and kinetochore localization domains of hZW10 remain unclear. We therefore set out to map the kinetochore localization domain of hZW10 by creating an extensive series of sequential N- and C-terminal deletion constructs of hZW10 (Fig. 1 A). These EGFP-tagged constructs were expressed in HEK293 cells and confirmed by Western blotting (Fig. S1, B and D, available at <http://www.jcb.org/cgi/content/full/jcb.200708021/DC1>). Analysis of expression levels revealed an approximately twofold overexpression of EGFP-hZW10 (Fig. S1 E). However, transient transfection often leads to a broad range of expression levels and, therefore, the overexpression of every construct was not determined. Presence of the EGFP fusions at kinetochores in transfected mitotic HeLa cells was determined using fluorescence microscopy in both prometaphase and metaphase (Fig. 1 B). To increase the sensitivity of the kinetochore localization assay, we also treated the transfected cells with vinblastine to eliminate kinetochore-MT attachment and thus enhance hZW10 kinetochore recruitment (Fig. S1 F). Our analysis indicated that the first 52 aa of hZW10 (mutant N1) are dispensable for kinetochore localization. Any N-terminal deletions larger than 52 aa, such as 75 aa (mutant N2), resulted in loss of kinetochore localization (Fig. 1 B and Fig. S1 A). The inability of deletion constructs (N2–9) to localize to kinetochores could reflect the loss of proper folding of the protein. Contrary to published results, we found that the N-terminal 82 aa of hZW10 (mutant C10) was not sufficient for kinetochore localization (Fig. 1 B; H. Wang et al., 2004). In fact, any deletion from the C terminus resulted in the loss of kinetochore localization (Fig. 1 B, Fig. S1 C, and Table I), thus indicating that the C terminus of hZW10 is essential for kinetochore localization. However, none of the C-terminal fragments of hZW10 (N5–9) were able to localize to kinetochores. Our deletion-mapping results therefore indicate that the N-terminal boundary for hZW10 kinetochore targeting is near aa 52, whereas the C-terminal boundary extends to the C terminus because no deletions from this end were tolerated.

for kinetochore localization during mitosis using fluorescence microscopy. Representative images show that insertion mutations in the C terminus of hZW10 (mutants R, U, and X) abolish kinetochore localization of hZW10. Fluorescence microscopy analysis of remaining constructs is shown in Fig. S4 A (available at <http://www.jcb.org/cgi/content/full/jcb.200708021/DC1>) and their kinetochore localization status is summarized in Table II. Chromosomes are stained with DAPI. Bar, 10 μ m. (e) HeLa cells transiently transfected with the EGFP-hZW10^{N1} pentapeptide insertion mutant constructs were analyzed for kinetochore localization during mitosis using fluorescence microscopy. Representative images show that peptide insertions in the C terminus of hZW10^{N1} (mutants N1^a, N1^b, and N1^c) abolish the ability of hZW10 to localize to the kinetochore. Fluorescence microscopy analysis of remaining constructs is shown in Fig. S5 A and their kinetochore localization status is summarized in Table II. Chromosomes are stained with DAPI. Bar, 10 μ m.

Table I. hZW10 N- and C-terminal truncation mutants assayed for kinetochore localization and hZwint-1 interaction

hZW10 construct	Encoding amino acids	Kinetochore localization	hZwint-1 yeast two-hybrid interaction	β -Galactosidase assay (\pm one SD)
Full length	1–779	Positive	Positive	187 \pm 20
N1	52–779	Positive	Negative	2.14 \pm 1.9
N2	75–779	Negative	Negative	ND
N3	85–779	Negative	Negative	ND
N4	132–779	Negative	Negative	ND
N5	215–779	Negative	Negative	ND
N6	335–779	Negative	Negative	ND
N7	462–779	Negative	Negative	ND
N8	556–779	Negative	Negative	ND
N9	621–779	Negative	Negative	ND
C1	1–772	Negative	Negative	3.4 \pm 0.9
C2	1–698	Negative	Negative	2.6 \pm 0.6
C3	1–560	Negative	Negative	2.5 \pm 0.8
C4	1–496	Negative	Negative	1.0 \pm 0.8
C5	1–410	Negative	Positive	26.6 \pm 3
C6	1–356	Negative	Positive	275 \pm 33
C7	1–318	Negative	Positive	132 \pm 62
C8	1–224	Negative	Positive	233 \pm 23
C9	1–139	Negative	Positive	445 \pm 128
C10	1–82	Negative	Positive	ND

The assay of direct interaction between hZwint-1 and hZW10 deletion constructs analyzed with the LexA yeast two-hybrid system using Xgal and the β -galactosidase assay, as well as kinetochore localization, through fluorescence microscopy analysis of EGFP fusion constructs. Yeast colonies were scored for appearance of blue color 2 and 3 d after streaking out. Each combination of interactions was redone in three separate experiments and confirmed for expression of fusion constructs by Western blotting with anti-HA and anti-LexA antibodies (not depicted). The β -galactosidase assay was performed using the β -galactosidase assay kit according to the manufacturer's instructions.

The interaction between hZW10 and hZwint-1 is dispensable for kinetochore localization of hZW10

hZW10 kinetochore localization has previously been correlated with hZwint-1 interaction using the yeast two-hybrid assay (H. Wang et al., 2004). We therefore analyzed our deletion mutant library for interaction with hZwint-1 using the Lex-A-based yeast two-hybrid assay (Toby and Golemis, 2001). Wild-type hZW10 and hZwint-1 readily interacted in the Lex-A-based yeast two-hybrid assay (Table I). When screening our truncation mutants, we found that all the N-terminal deletion constructs (N1–9) as well as the C-terminal truncations C1–4 lost the ability to interact with hZwint-1. However, constructs C5–10, which all lack at least the C-terminal third of hZW10 (aa 410–779), retained the ability to interact with hZwint-1 (Fig. 1 A and Table I). The smallest N-terminal fragment of hZW10, which retained the ability to interact with hZwint-1, was C10, aa 1–82 (Table I). We therefore concluded that the N terminus of hZW10 (aa 1–82) contains the hZwint-1 interaction domain. Interestingly, our results also indicated that the direct interaction between hZW10 and hZwint-1, in the context of the entire protein, requires the C terminus (aa 410–779). Mutants C1–4, although containing the hZwint-1 interaction domain (aa 1–82), did not interact with hZwint-1. These findings may reflect that mutants C1–4 have incorrect folding. To narrow down the N-terminal boundary for the hZwint-1 interaction domain, we also generated several smaller deletions of hZW10 (Fig. S2 A, available at <http://www.jcb.org/cgi/content/full/jcb.200708021/DC1>).

We found that N-terminal deletions of more than 30 aa disrupted the hZW10–hZwint-1 interaction (Fig. S2 A). These findings narrow down the hZwint-1 interaction domain of hZW10 to aa 30–80. All the constructs with N-terminal deletions \leq 52 aa retained the ability to localize to kinetochores (Fig. S2, B and C). More importantly, mutant C10, which contains the proposed kinetochore localization domain (H. Wang et al., 2004) of hZW10, did not localize to kinetochores in our experiments. We therefore conclude that the N terminus of hZW10 is indeed sufficient for hZwint-1 interaction but is not sufficient for kinetochore localization. Our results indicate that the hZW10–hZwint-1 interaction may be dispensable for hZW10 kinetochore recruitment.

To confirm our yeast two-hybrid results, we performed in vitro GST pulldown experiments using GST–hZwint-1 to assay for interaction with EGFP-hZW10 or EGFP-hZW10^{N1}. We observed that GST–hZwint-1 readily pulled down EGFP-hZW10 from HEK293 cell lysates cotransfected with the GST–hZwint-1 and EGFP-hZW10 constructs (Fig. S2 D). In contrast, when GST–hZwint-1 was used to pull down EGFP-hZW10^{N1}, we observed a markedly reduced amount of EGFP-hZW10^{N1} associated with GST–hZwint-1 compared with that of EGFP-hZW10. Other hZwint-1–noninteracting mutants behaved similarly to N1 when analyzed by the GST pulldown assay (Fig. S2 E). These results suggest that the hZwint-1–noninteracting hZW10 mutants that were identified using the yeast two-hybrid assay also do not interact with hZwint-1 in mammalian tissue culture cells.

Table II. hZW10 and N1 insertion mutants assayed for kinetochore localization and hZwint-1 interaction

hZW10 mutant	Insertion site (amino acid)	Insertion sequence (amino acid) ^a	Kinetochore localization	hZwint-1 yeast two-hybrid interaction	β-Galactosidase assay (± one SD) ^b
A	43	CGRIS	Positive	Positive	341 ± 173
B	61	VRPHQ	Positive	Negative	1.3 ± 0.3
C	90	CGRTG	Positive	Positive	333 ± 114
D	106	CGRIL	Positive	Positive	ND
E	131	CGRKY	Positive	Positive	ND
F	191	LRPQP	Positive	Positive	ND
G	208	CGRNL	Positive	Positive	ND
H	210	VRPHT	Positive	Positive	ND
I	226	VRPHS	Positive	Positive	ND
J	248	LRPQL	Negative	Negative	ND
K	335	VRPHW	Positive	Positive	ND
L	375	NAAAL	Positive	Positive	ND
M	421	CGRNN	Positive	Positive	ND
N	467	DAAAL	Positive	Positive	ND
O	475	TAAAP	Positive	Positive	ND
P	536	LRPHQ	Negative	Negative	9.9 ± 9.6
Q	563	CGRSL	Positive	Positive	ND
R	583	CGRRR	Negative	Negative	2.4 ± 0.7
S	607	SAAAAA	Positive	Positive	ND
T	608	MRPHR	Positive	Positive	ND
U	654	CGRMG	Negative	Negative	3.7 ± 1.6
V	663	CGRTE	Negative	Negative	2.2 ± 0.9
W	666	CGRIG	Negative	Negative	1.6 ± 0.7
X	671	CGRTL	Negative	Negative	2.1 ± 1.7
Y	682	LRPQL	Positive	Positive	ND
Z	686	CGRIC	Negative	Negative	1.4 ± 0.8
Aa	712	CGRKE	Positive	Positive	ND
a	149	SMRPQ	Positive	N/A	N/A
b	210	TECGR	Positive	N/A	N/A
c	235	CGRIG	Positive	N/A	N/A
d	283	LVFKH	Positive	N/A	N/A
e	289	PCLNT	Positive	N/A	N/A
f	303	QMRPH	Positive	N/A	N/A
g	331	AAALG	Positive	N/A	N/A
h	334	CLNTN	Positive	N/A	N/A
i	390	NAAAL	Positive	N/A	N/A
j	454	LRPHQ	Positive	N/A	N/A
k	520	HVFKH	Positive	N/A	N/A
l	541	CFGIH	Positive	N/A	N/A
m	567	LFKHL	Positive	N/A	N/A
n	640	CLMNW	Negative	N/A	N/A
o	658	AAALN	Negative	N/A	N/A
p	675	TVFKH	Negative	N/A	N/A
q	681	LLRPQ	Positive	N/A	N/A

The assay of direct interactions between hZwint-1 and hZW10 insertion constructs analyzed with the LexA yeast two-hybrid system using Xgal and the β-galactosidase assay, as well as kinetochore localization, through fluorescence microscopy analysis of EGFP fusion constructs.

^aThe exact amino acid insertion sites in hZW10 and hZW10^{N1} 5-aa insertion mutants were determined by sequencing.

^bThe hZwint-1 interaction with hZW10 insertion mutants were assayed as outlined in Table I.

The hZW10 kinetochore localization domain resides within the C terminus

To further define the kinetochore localization and hZwint-1 interaction domains of hZW10, we used a random insertion mutagenesis approach. A library of hZW10 insertion mutants were created using transposon-based insertion mutagenesis, where 15 bp were randomly inserted into the hZW10 or N1 cDNA.

We selected an array of 27 insertion mutants spanning the hZW10 cDNA and 17 insertion mutants spanning the N1 cDNA for functional analysis (Fig. 1 C and Table II). Fluorescence microscopy of HeLa cells transfected with EGFP fusion insertion mutant constructs identified several kinetochore nonlocalizing mutants, the majority of which were confined to the C terminus of the hZW10 and N1 cDNAs (Table II). Fig. 1 D shows representative

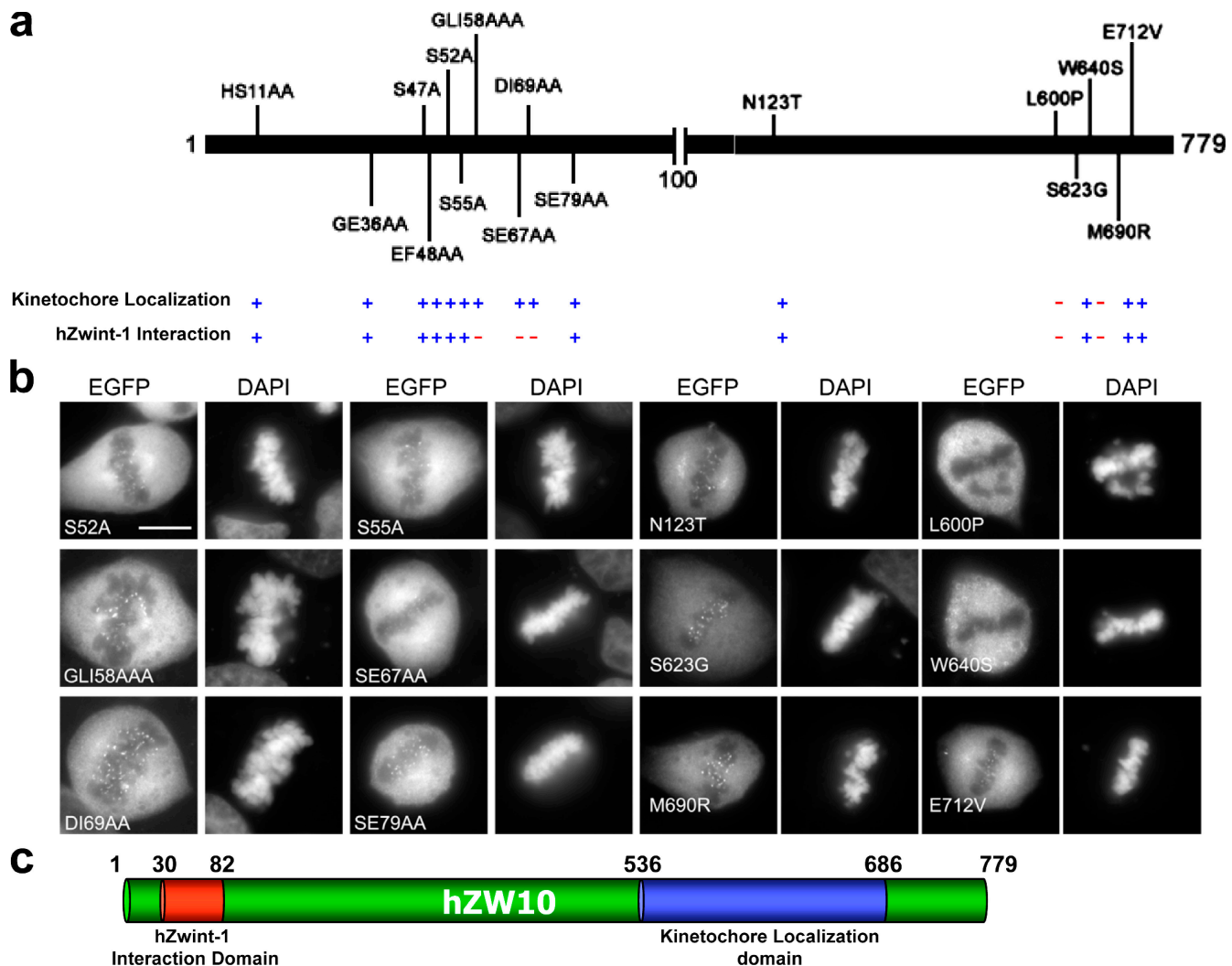


Figure 2. hZW10 domains specifying hZwint-1 interaction and kinetochore localization are distinct. (a) A schematic diagram of hZW10 depicting single amino acid changes generated in this study. Conservation of the amino acids chosen for mutagenesis is shown in Figs. S3 (A and B, available at <http://www.jcb.org/cgi/content/full/jcb.200708021/DC1>) and S4 (A and B). Yeast two-hybrid interaction with hZwint-1 and kinetochore localization are indicated by a blue plus sign for positive interaction and a red minus sign for negative interaction. (b) HeLa cells transiently transfected with the EGFP-hZW10 site-directed mutant constructs were analyzed for kinetochore localization during mitosis using fluorescence microscopy. Representative images show that none of the hZW10 N-terminal mutants interfere with hZW10 localization at kinetochores. Mutations L600P and W640S abolish hZW10 localization at kinetochores. Analysis of all remaining amino acid substitution mutant constructs is shown in Figs. S3 (A and B) and S4 (A and B). All mutants behaved similarly at both prometaphase and metaphase kinetochores. Bar, 10 μ m. (c) A model diagram of hZW10 functional domains mapped by the mutagenesis screen. The N terminus of hZW10 (aa 30–80) contains the direct hZwint-1 interaction domain of hZW10, whereas the C terminus (aa 536–686) contains the kinetochore localization domain.

hZW10 insertion mutants (R, U, and X) that did not localize to kinetochores as well as insertion mutants that retained the ability to localize (B, F, and Aa). Fig. 1 E shows representative N1 insertion mutants that were unable to localize to kinetochores (N1ⁿ, N1^o, and N1^p) as well as N1 insertion mutants that did localize (N1^a, N1^m, and N1^q). Analysis of all the remaining insertion mutants is presented in Figs. S3 A and S4 A (available at <http://www.jcb.org/cgi/content/full/jcb.200708021/DC1>) and summarized in Table II. Again, the kinetochore nonlocalizing mutants were confirmed for loss of localization in cells lacking kinetochore-MT attachments (Figs. S3 B and S4 B). The insertion mutagenesis thus confirmed our deletion library results in that the C terminus of hZW10 (aa 536–686) is essential for its kinetochore localization.

The insertion mutants were also assayed for interaction with hZwint-1 using the yeast two-hybrid assay. In concordance with our deletion analysis, we identified an N-terminal hZW10 insertion mutant occurring within the hZwint-1 interaction domain that no longer interacted with hZwint-1 (Table II, mutant B, insertion at aa 61). The lack of interaction with hZwint-1 was again confirmed by GST pulldown (Fig. S2 E). This particular insertion mutant still localized to kinetochores when analyzed by fluorescence microscopy (Fig. 1 D and S3 B). We also found that C-terminal insertion mutants that did not localize to the kinetochore also did not interact with hZwint-1 (Fig. 1 C and Table II). These insertion mutations (P, R, U, V, W, X, and Z) occurred between aa 536 and 686. The results from these C-terminal insertion mutants were surprising

because the deletion analysis we had performed identified the N terminus of hZW10 (aa 30–80) as the hZwint-1 interaction domain. We therefore conclude that the C terminus of hZW10 may play an indirect role in the interaction between hZwint-1 and hZW10.

To further validate our insertion mutagenesis results, we generated several single or multiple amino acid substitutions within the hZW10 cDNA, specifically at the C and N termini. These mutations were designed, based on our insertion mutagenesis screen, to specifically disrupt the hZwint-1 interaction and/or kinetochore localization domains of hZW10 (Fig. 2 A). In addition, we generated two mutations of hZW10 that have been reported in colon cancer, N123T and S623G (Z. Wang et al., 2004). Fluorescence microscopy analysis of HeLa cells transiently transfected with the mutant constructs revealed that two of our C-terminal hZW10 point mutants, L600P and W640S, no longer localized to kinetochores (Fig. 2 B and Fig. S5 C, available at <http://www.jcb.org/cgi/content/full/jcb.200708021/DC1>). These mutants further confirmed our finding that the kinetochore localization domain of hZW10 resides within the C terminus. In addition, we isolated three N-terminal mutants, GLI58AAA, SE67AA, and DI69AA, that did not interact with hZwint-1 in the yeast two-hybrid assay or the GST pulldown assay yet retained kinetochore localization (Fig. 2, Fig. S2 E, Fig. S5 F, and Table III). These mutants further confirmed that the N terminus of hZW10 contains the hZwint-1 interaction domain and that hZwint-1 interaction is dispensable for hZW10 kinetochore localization. Lastly, we found that the two colon cancer-associated point mutations had no effect on the ability of hZW10 to localize to kinetochores or interact with hZwint-1 (Fig. 2).

Based on our extensive mutagenesis screen of hZW10 for the kinetochore localization and hZwint-1 interaction domain, we conclude that hZW10 contains two separate functional domains (Fig. 2 C). hZW10 directly interacts with hZwint-1 through an N-terminal domain (aa 30–80), whereas it localizes to kinetochores through a C-terminal domain (aa 536–686). The C-terminal domain of hZW10 alone, however, is not sufficient for kinetochore localization and the entire protein is likely to be required for proper function. Our conclusions as to the kinetochore localization domain boundaries are made largely based on our insertion and amino acid substitution mutagenesis results. The deletion mutations were not informative and likely did not behave properly *in vivo* because of problems with folding. As such, we have been unable to isolate a kinetochore localization domain away from the rest of the protein. Although hZwint-1 has been proposed to be required for hZW10 kinetochore localization, we find that disruption of the hZW10–hZwint-1 interaction does not prevent hZW10 kinetochore localization.

hZW10 residency at the kinetochore is influenced by kinetochore-MT attachment as well as the interaction between hZW10 and hZwint-1

Many of the mitotic checkpoint proteins required for generating the wait anaphase signal are known to be dynamic components of the kinetochore. Mad2, the quintessential component

Table III. hZW10 N-terminal point mutants analyzed for kinetochore localization and hZwint-1 interaction

hZW10 point mutation ^a	Kinetochore localization	hZwint-1 yeast two-hybrid interaction	β-Galactosidase assay (± one SD) ^b
HS11AA	Positive	Positive	ND
GE36AA	Positive	Positive	ND
S47A	Positive	Positive	ND
EF48AA	Positive	Positive	ND
S52A	Positive	Positive	ND
S55A	Positive	Positive	449 ± 139
GLI58AAA	Positive	Negative	2.7 ± 0.8
SE67AA	Positive	Negative	1.8 ± 0.9
DI69AA	Positive	Negative	1.2 ± 0.4
SE79AA	Positive	Positive	131 ± 41

The assay of direct interactions between hZwint-1 and hZW10 site-directed mutagenesis constructs analyzed with the LexA yeast two-hybrid system using Xgal and the β-galactosidase assay, as well as kinetochore localization, through fluorescence microscopy analysis of EGFP fusion constructs.

^aThe point mutations were verified by sequencing.

^bThe hZwint-1 interaction with hZW10 point mutants were assayed as outlined in Table I.

of the mitotic checkpoint, is known to be highly dynamic at unattached kinetochores (Shah et al., 2004). FRAP experiments have shown that Mad2 has a $t_{1/2}$, the time required for 50% recovery of fluorescence signal, of 4–5 s (Shah et al., 2004). Mps1, Cdc20, hBubR1, and hBub3 have also been shown to be dynamic components of the kinetochore (Howell et al., 2004). In contrast, structural components of the mitotic checkpoint, such as hHec1 and hNuf2, have been shown to be stable components of kinetochores (Hori et al., 2003). ZW10 and ROD, both essential components of the mitotic checkpoint thought to be involved in checkpoint signaling, may also be dynamic components of kinetochores. Studies using a GFP-tagged dmROD have shown that dmROD is in fact a dynamic component of the kinetochore with a $t_{1/2}$ recovery time of 25–45 s in prometaphase (Basto et al., 2004). However, kinetochore dynamics for dmZW10 or hZW10 remain unexamined.

To analyze hZW10 kinetochore dynamics, we generated a HeLa cell line stably expressing EGFP-hZW10. This cell line was subsequently used for FRAP experiments. We analyzed EGFP-hZW10 turnover at single kinetochores during different stages of mitosis. At the prometaphase kinetochore, we observed very little turnover of EGFP-hZW10 (Fig. 3 A). This suggested that EGFP-hZW10 remains stably bound to kinetochores that have not achieved metaphase alignment. At the metaphase kinetochore, we observed rapid turnover of EGFP-hZW10 with a $t_{1/2}$ recovery of 13.8 ± 5.2 s (Fig. 3 A). This suggested that hZW10 becomes a dynamic component of the kinetochore once bipolar kinetochore–MT attachment occurs. To verify our prometaphase results, we also analyzed the turnover rate of EGFP-hZW10 in cells treated with 7 μM STLC, a small molecule inhibitor of the kinesin Eg5 that results in monopolar spindles (Skoufias et al., 2006). Similar to prometaphase, we observed no turnover of EGFP-hZW10 in these cells (Fig. S4 D). Furthermore, we used 0.1 μM vinblastine to inhibit spindle formation and, therefore, prevent any MT occupancy at kinetochores (Jordan et al., 1992).

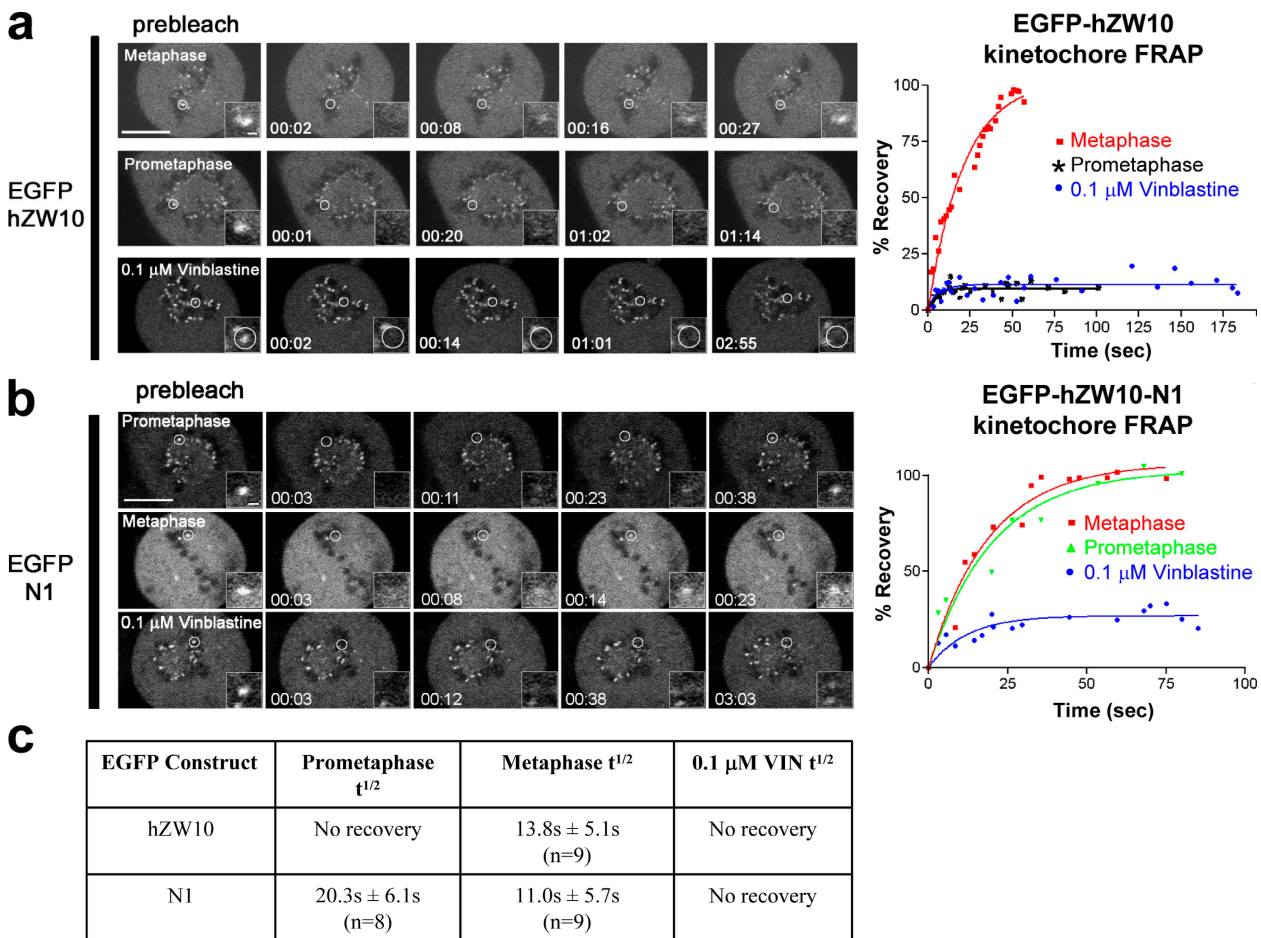


Figure 3. hZW10 kinetochore dynamics are regulated by kinetochore–MTs and interaction with hZwint-1. (a) Time-lapse series showing EGFP-hZW10 recovery after photobleaching at single kinetochores in metaphase (top), prometaphase (middle), or in cells treated with 0.1 μM vinblastine (bottom). The time scale is in minutes:seconds and the kinetochores that were bleached are outlined by white circles and enlarged at the bottom right. Bars: (large) 10 μm; (small) 1 μm. Nonlinear regression curves of percent recovery of the EGFP-hZW10 kinetochore signal from the time of photobleaching are shown at the right. (b) Time-lapse series showing EGFP-hZW10^{N1} recovery after photobleaching at single kinetochores in metaphase (middle), prometaphase (top), or in cells treated with 0.1 μM vinblastine (bottom). The time scale is in minutes:seconds and the kinetochores that were bleached are outlined by white circles and enlarged in the bottom right. Bars: (large) 10 μm; (small) 1 μm. Nonlinear regression curves of percent recovery of the EGFP-hZW10 kinetochore signal from the time of photobleaching are shown on the right. (c) Numerical summary of kinetochore $t_{1/2}$ values obtained from FRAP experiments performed on the EGFP-hZW10– and EGFP-hZW10^{N1}–expressing cells.

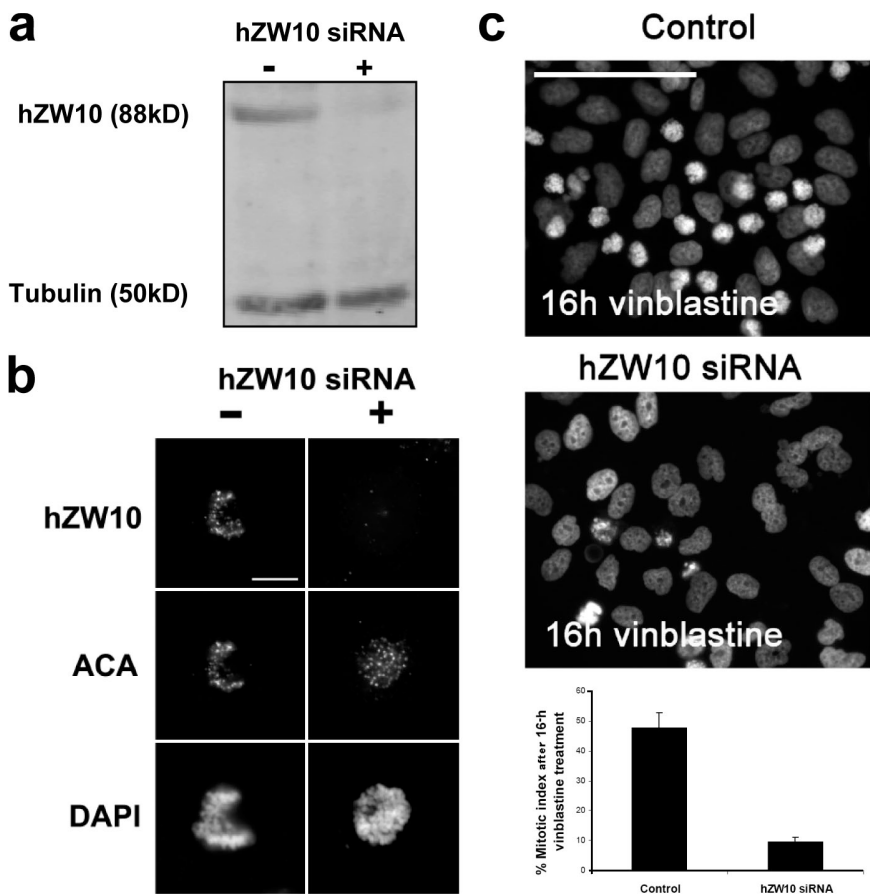
The vinblastine treatment also resulted in the stabilization of EGFP-hZW10 at kinetochores with little to no observable turnover (Fig. 3 A). The table in Fig. 3 C summarizes the $t_{1/2}$ recovery measurements for EGFP-hZW10. Based on the FRAP data, we conclude that hZW10 turnover at the kinetochore occurs only when chromosomes achieve bipolar kinetochore–MT attachments.

We have determined that the N1 hZW10 deletion construct does not interact with hZwint-1 but does localize to kinetochores. We therefore used EGFP-hZW10^{N1} to determine whether the loss of hZwint-1 interaction can alter hZW10 kinetochore dynamics. We generated a HeLa cell line stably expressing the EGFP-hZW10^{N1} and analyzed EGFP-hZW10^{N1} kinetochore turnover by FRAP. Unlike the full-length EGFP-hZW10 fusion construct, we observed EGFP-hZW10^{N1} turnover at pro-metaphase kinetochores. EGFP-hZW10^{N1} kinetochore turnover at prometaphase had a $t_{1/2}$ of 20 ± 5 s ($n = 9$; Fig. 3 B). EGFP-hZW10^{N1} also turned over in cells arrested with monopolar spindles (Fig. S4 D). EGFP-hZW10^{N1} kinetochore turnover

during metaphase had a $t_{1/2}$ recovery of 11.0 ± 5.7 s ($n = 8$), which is similar to that of full-length EGFP-hZW10 (Fig. 3 B). 0.1-μM vinblastine treatments of EGFP-hZW10^{N1}–expressing cells resulted in stabilization of EGFP-N1 at kinetochores, indicating that kinetochore–MT attachments, although not necessarily bipolar, are still required for EGFP-hZW10^{N1} kinetochore turnover (Fig. 3 B, bottom). The table in Fig. 3 C summarizes the $t_{1/2}$ recovery measurements for EGFP-hZW10^{N1} compared with those of wild-type EGFP-hZW10. The temporal pattern of EGFP-hZW10 kinetochore turnover, which we have determined depends on bipolar kinetochore–MT attachments, is, therefore, also functionally regulated by the interaction of hZW10 with hZwint-1.

hZwint-1 regulation of hZW10 kinetochore dynamics is required for fidelity of the mitotic checkpoint

hZW10 has been shown to be required for mitotic checkpoint fidelity in fly, frog, and human cells (Williams et al., 1992; Basto



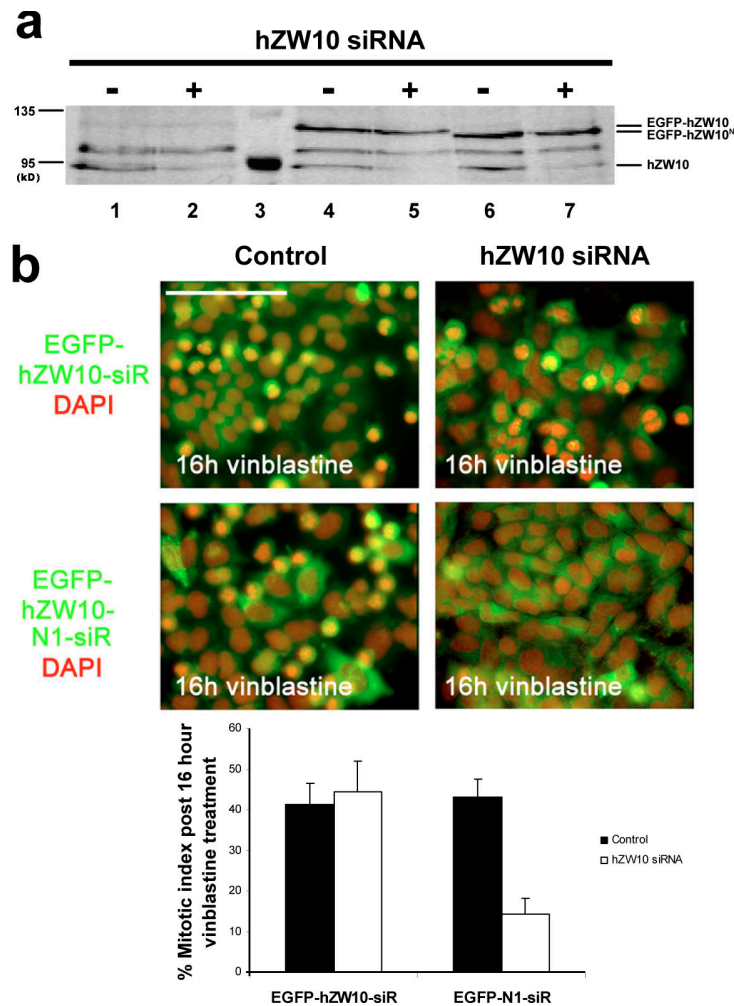
et al., 2000; Chan et al., 2000; Scaerou et al., 2001; Kops et al., 2005). We therefore investigated whether the interaction between hZW10 and hZwint-1, which we have shown to regulate hZW10 kinetochore dynamics in prometaphase, is functionally required for mitotic checkpoint fidelity. To assess the fidelity of the mitotic checkpoint in the presence of an hZwint-1–non-interacting hZW10 mutant, endogenous hZW10 was depleted by siRNA while the cells were rescued with either a wild-type EGFP-hZW10 or EGFP-hZW10^{N1} siRNA-resistant construct. Fig. 4 A depicts the knockdown of endogenous hZW10 protein by immunoblot, whereas Fig. 4 B illustrates immunofluorescence staining for hZW10 siRNA knockdown. In either case, hZW10 is clearly depleted after 72 h of siRNA transfection. To assay mitotic checkpoint function in cells lacking hZW10, cells depleted of hZW10 using siRNA for 72 h were arrested with vinblastine for 16 h and analyzed using fluorescence microscopy. In control cells, the vinblastine-induced mitotic arrest resulted in a mitotic index of ~45% (Fig. 4 C). However, in cells knocked down for hZW10 and subsequently arrested with vinblastine, the mitotic index dropped to ~10%, thus indicating escape from mitotic checkpoint arrest (Fig. 4 C). To test whether EGFP-hZW10 or EGFP-hZW10^{N1} can rescue the hZW10 siRNA knockdown phenotype, we generated HeLa cell lines stably expressing EGFP-hZW10 or EGFP-hZW10^{N1} siRNA-resistant constructs. We subsequently depleted endogenous hZW10 in the siRNA-resistant cell lines for 72 h, arrested the cells with vinblastine for 16 h, and analyzed using fluorescence microscopy.

Fig. 5 A shows the depletion of endogenous hZW10 protein and the expression of EGFP-hZW10 siRNA-resistant constructs. In control cells expressing either siRNA-resistant EGFP-hZW10 or EGFP-hZW10^{N1}, the vinblastine-induced mitotic arrest resulted in a mitotic index of ~42 and 43%, respectively. However, when we depleted endogenous hZW10, the EGFP-hZW10^{N1}-expressing cells reached a mitotic index of only ~16%, whereas the mitotic index of the EGFP-hZW10-expressing cells reached ~45%, which was similar to the control HeLa cells (Figs. 4 and 5). In conclusion, our results indicate that although wild-type EGFP-hZW10 can rescue the depletion of endogenous hZW10, EGFP-hZW10^{N1} is unable to support a sustained mitotic checkpoint arrest in response to vinblastine treatment. We therefore believe that the interaction between hZW10 and hZwint-1, which stabilizes hZW10 at prometaphase kinetochores, is required for mitotic checkpoint fidelity.

Discussion

In our current study, we have applied a structure function assay to map the kinetochore localization and hZwint-1 interaction domains of hZW10. In addition, we have documented the kinetochore dynamics of hZW10 during prometaphase and metaphase, observing that kinetochore hZW10 becomes dynamic only upon metaphase alignment. We discovered that hZW10 kinetochore dynamics are regulated by kinetochore–MT attachments and the interaction between hZW10 and hZwint-1. We found that although

Figure 5. Interaction of hZW10 with hZwint-1 is required for the mitotic checkpoint. (a) Immunoblot of HeLa cells, HeLa cells stably expressing the EGFP-hZW10 siRNA-resistant construct, or HeLa cells stably expressing the EGFP-hZW10^{N1} siRNA-resistant constructs, all of which were transfected with hZW10 siRNA for 72 h and probed with rabbit polyclonal antibodies against hZW10. Lanes 1 and 2 are control HeLa cells; lane 3 is the molecular mass marker; lanes 4 and 5 are the EGFP-hZW10 stable cell line; and lanes 6 and 7 are the EGFP-hZW10^{N1} stable cell line. Endogenous hZW10 is clearly knocked down, whereas the siRNA-resistant EGFP constructs remain. (b) Representative images of HeLa cells stably expressing EGFP-hZW10 or EGFP-hZW10^{N1} arrested with 25 μ M vinblastine for 16 h or transfected with anti-hZW10 siRNA duplexes for 72 h and arrested with 25 μ M vinblastine for 16 h. EGFP-hZW10-siR– or EGFP-N1-siR-expressing cells were analyzed for the accumulation of mitotic cells by the staining of their DNA with DAPI. Bar, 100 μ m. A histogram of the percentage of mitotic cells is shown ($n = 3$; >300 cells per experiment; error bars show \pm SD).



the hZwint-1 interaction is dispensable for hZW10 kinetochore recruitment, it is essential for the stabilization of hZW10 residency at prometaphase kinetochores and mitotic checkpoint function.

Using our extensive mutant library of hZW10, we found that hZW10 contains two functional domains, one within the C terminus (aa 536–686) and the other at the extreme N terminus (aa 30–82). We mapped the kinetochore localization domain of hZW10 to the C terminus and the hZwint-1 interaction domain to the N terminus (Fig. 2C). Both domains are highly conserved in vertebrates (Fig. S5, A and D). Interestingly, the C-terminal kinetochore localization domain alone is not sufficient to confer hZW10 kinetochore localization. We therefore hypothesize that hZW10 kinetochore localization may require an interaction between the C and N termini of hZW10. We have attempted to analyze an interaction between the two termini using a yeast two-hybrid approach; however, we have been unsuccessful as of yet. Further biochemical experiments are thus required to thoroughly test our hypothesis. Because our domain mapping results are largely based on yeast two-hybrid assays, we cannot rule out the possibility that these mutants may interact differently at kinetochores *in situ*. However, based on the sum of all our different mutants, including truncations, insertion, and site-directed mutants, we are confident in the accuracy of the mapped kinetochore localization and hZwint-1 interaction domains of hZW10. The location

of hZW10 interaction domains for dynamitin and hROD remains unknown at this time; however, Starr et al. (1998) mapped the dynamitin interaction domain to the C terminus of hZW10 (aa 468–779). Taking into account the mapping by Starr et al. (1998) in combination with our hZW10 C-terminal mutant results, it remains possible that the interaction between hZW10 and dynamitin may also play a role in hZW10 kinetochore localization. Because hZW10 and hROD are interdependent for kinetochore localization (Chan et al., 2000), the interaction between hZW10 and hROD may also be required for hZW10 kinetochore localization as part of the RZZ complex.

Although H. Wang et al. (2004) had previously correlated hZW10 kinetochore localization with hZwint-1 interaction, we have found that specific disruption of the hZwint-1 interaction domain, via deletion, insertion, or amino acid substitution, does not preclude hZW10 kinetochore localization. Based on our data, we propose that the hZW10 kinetochore recruitment mechanism may not directly depend on hZwint-1. Using our hZW10 mutant library, we mapped the hZwint-1 interaction domain of hZW10 to its N terminus (aa 30–80). In addition, we have found that the interaction between hZW10 and hZwint-1, in context of the entire protein, also involves the C terminus of hZW10 (aa 410–779). Although previous siRNA-mediated knockdown of hZwint-1 has clearly shown the loss of hZW10 from kinetochores, our

study shows that the loss of direct interaction between hZwint-1 and hZW10 does not affect hZW10 kinetochore localization. hZwint-1 is known to interact with the Ndc80 and Mis12 complexes, which are essential for the assembly of functional kinetochores (Cheeseman et al., 2004; Obuse et al., 2004; Lin et al., 2006). The absence of hZwint-1 may therefore indirectly affect hZW10 kinetochore localization by preventing or altering kinetochore assembly through the disruption of the Ndc80 and/or Mis12 complexes. It has been suggested that the RZZ complex oligomerizes at kinetochores (Scaerou et al., 2001). RZZ complex oligomerization at kinetochores may therefore represent an alternate hZW10 kinetochore recruitment mechanism. Interestingly, we have observed the dimerization of EGFP-hZW10 with GST-hZW10 using in vitro GST pulldown assays (Fig. S2 F). We cannot, therefore, rule out the possibility that endogenous hZW10 facilitates the recruitment of hZwint-1–noninteracting hZW10 proteins to kinetochores. We do observe the localization of EGFP-hZW10^{N1} at kinetochores in a subset of cells depleted of endogenous hZW10; however, we cannot determine whether endogenous hZW10 has been completely eliminated from these cells (unpublished data). The initial recruitment of hZW10 to kinetochores during early prometaphase may depend on hZwint-1; however, the dynamic recruitment of kinetochore hZW10 throughout the remainder of mitosis is hZwint-1 independent. Future studies of hZW10, hROD, and hZwilch will need to focus on RZZ complex dimerization in relation to kinetochore localization and its function within the mitotic checkpoint.

In addition to our findings that the hZwint-1 interaction is dispensable for hZW10 kinetochore localization, we have also discovered that hZwint-1 modulates hZW10 kinetochore dynamics. In Fig. 6, we outline a model whereby hZW10 kinetochore turnover is regulated by bipolar kinetochore–MT attachments as well as by interaction with hZwint-1. Using FRAP experiments with HeLa cells stably expressing EGFP-hZW10, we have established that hZW10 kinetochore dynamics are regulated by bipolar kinetochore–MT attachments. At prometaphase kinetochores EGFP-hZW10 is stable; however, once bipolar kinetochore–MT attachments are achieved and the chromosomes align at the metaphase plate, EGFP-hZW10 becomes highly dynamic. We therefore believe that the observed hZW10 accumulation at prometaphase or nocodazole-treated kinetochores (Starr et al., 1997) stems from its inability to turn over at kinetochores lacking proper kinetochore–MT attachments (Fig. 6 A). In contrast, hZW10 diminishes at metaphase kinetochores because its kinetochore turnover rate becomes rapid upon the establishment of metaphase alignment (Fig. 6 B). In our model, we predict that the turnover of kinetochore hZW10 depends on its transport off kinetochores and along kinetochore–MTs mediated by dynein/dynactin. This explains why both the wild-type hZW10 and the hZW10^{N1} mutant do not turn over at kinetochores in vinblastine-treated cells. In the vinblastine-treated cells, no kinetochore–MTs are present and, therefore, dynein/dynactin-mediated transport of hZW10 off kinetochores is not possible. Interestingly, our results contrast those of Basto et al. (2004), who found GFP-dmROD to be dynamic at prometaphase and colchicine-treated kinetochores in live *D. melanogaster* embryos. We attribute this difference to two factors. First, early-stage embryos undergo very rapid cell

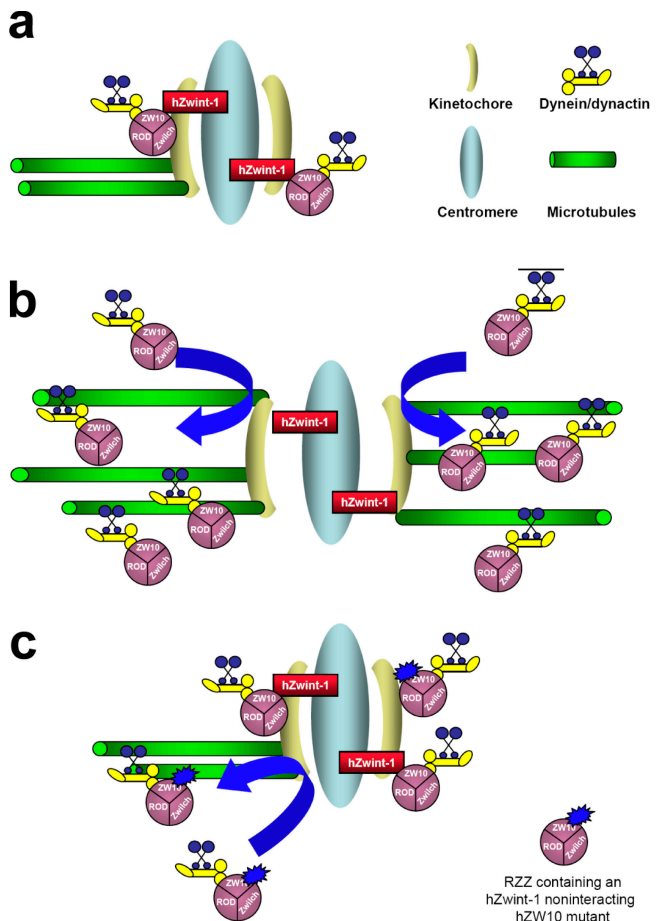


Figure 6. Model of the mechanisms regulating hZW10 kinetochore dynamics. (a) hZW10, as part of the RZZ complex, localizes to prometaphase and/or unattached kinetochores where it interacts with hZwint-1. The RZZ complex recruits dynein/dynactin to the kinetochore. The RZZ complex remains stably bound to the kinetochore, via the interaction with hZwint-1, until bipolar kinetochore–MT attachments are achieved. The retention of hZW10 and, therefore, dynein/dynactin at kinetochores prevents premature silencing of the mitotic checkpoint. (b) At metaphase, when kinetochores have achieved bipolar kinetochore–MT attachments and the chromosomes have aligned at the metaphase plate, hZwint-1 no longer stabilizes hZW10 at kinetochores. Dynein/dynactin is now free to transport the RZZ complex off kinetochores, leading to silencing of the mitotic checkpoint. The RZZ complex continues to cycle on and off the kinetochore with very rapid dynamics to further facilitate removal of remaining checkpoint proteins such as hMad1 and 2. (c) RZZ complexes containing an hZwint-1–noninteracting mutant of hZW10 localize to kinetochores in prometaphase but do not remain stably bound and turn over at prometaphase kinetochores. These RZZ complexes still depend on the presence of kinetochore–MTs in order for dynein/dynactin-mediated transport off kinetochores but no longer require bipolar kinetochore attachment or the alignment of chromosomes to rapidly turn over at kinetochores. Premature removal of hZW10 from unaligned kinetochores leads to mitotic checkpoint failure.

divisions, thus requiring a short mitosis. The dynamics of the RZZ complex may therefore remain unregulated to allow a rapid release of checkpoint proteins from kinetochores, therefore driving quicker anaphase entry. Second, no hZwint-1 homologue has been found in flies. This could suggest that although the fly RZZ complex is dynamic at all kinetochores, human cells regulate the dynamics of the RZZ complex through its interaction with hZwint-1. The regulation of RZZ dynamics in human cells may indicate a need for a more intricate control of chromosome segregation.

hZW10 is the first example of a mitotic checkpoint protein displaying kinetochore turnover that depends on bipolar kinetochore–MT attachments. Moreover, when analyzing the kinetochore turnover of EGFP-*hZW10*^{N1}, an *hZwint-1*-noninteracting *hZW10* mutant, we observed kinetochore turnover at both prometaphase and metaphase kinetochores. Similar FRAP results were obtained using transient transfection of the DI69AA mutant, a site-directed mutant of *hZW10* that also does not interact with *hZwint-1* (unpublished data). This indicates that regulation of *hZW10* kinetochore turnover between prometaphase and metaphase requires the interaction between *hZW10* and *hZwint-1*. Kinetochore *hZwint-1* thus functions to increase the residency time of *hZW10* at kinetochores until bipolar MT attachments are achieved (Fig. 6 C). Once bipolar kinetochore attachments are achieved, *hZW10* is released from *hZwint-1* and becomes dynamic at kinetochores, leading to its transport off kinetochores by dynein/dynactin. The release of *hZW10* from *hZwint-1* in response to bipolar kinetochore–MT attachment may occur through posttranslational modifications of either *hZwint-1* or *hZW10*; however, the mechanism regulating this event remains unknown. In addition, we have observed that the fidelity of the mitotic checkpoint is compromised in the presence of EGFP-*hZW10*^{N1} and in the absence of endogenous *hZW10*. This loss of checkpoint fidelity stems from the inability of EGFP-*hZW10*^{N1} to stably bind prometaphase kinetochores, thus indicating that *hZwint-1*-mediated stabilization of *hZW10* residency at prometaphase kinetochores is essential for mitotic checkpoint function. Our findings support the hypothesis that dynein/dynactin-mediated transport of checkpoint proteins, such as *hZW10*, off kinetochores functions to silence the mitotic checkpoint and that this mechanism requires tight regulation to maintain checkpoint arrest.

In conclusion, we hypothesize that increased kinetochore residency of *hZW10* is required for maintenance of mitotic checkpoint signaling in response to unattached or monopolar attached kinetochore–MTs. Once metaphase alignment is achieved, *hZwint-1* no longer stabilizes *hZW10* at kinetochores and dynein/dynactin-dependent transport of *hZW10* along kinetochore–MTs results in a rapid kinetochore turnover rate of *hZW10*. We propose that *hZW10* kinetochore turnover acts as an indicator for the progression from prometaphase to metaphase, which is also indicative of the establishment of bipolar kinetochore–MT attachments. The fact that rapid turnover of *hZW10* is only observed at attached kinetochores, kinetochores that have satisfied the mitotic checkpoint, also supports the hypothesis that dynein/dynactin-mediated transport of *hZW10* silences the mitotic checkpoint (Musacchio and Salmon, 2007). Our findings thus indicate that mitotic checkpoint regulation involves a dynamic process at kinetochores rather than a simple on/off status of key mitotic checkpoint proteins at kinetochores. This study also highlights the need to study the kinetics of mitotic checkpoint protein accumulation at kinetochores *in vivo*.

Materials and methods

Cloning

hZW10 and *hZwint-1* cDNAs were amplified from a HeLa cDNA library (Clontech Laboratories, Inc.) using specific primers and cloned into the

pENTR vector (Invitrogen). *hZW10* N- and C-terminal deletion constructs (N1–9, C1–4, and C8–10) were amplified from the pENTR-*hZW10* vector using specific primers and cloned into pENTR. *hZW10* C-terminal deletions (C5–7) were cloned into the pDONR vector (Invitrogen) using attB recombination linkers for the Gateway Technology cloning system (Invitrogen). Cloning into expression vectors was performed using the Gateway Technology cloning system. The expression vectors used were Gateway destination vectors of pEGFP, pCG, pJG4-5, and pEG202 (Chan et al., 1998).

Mutagenesis

hZW10 insertion mutagenesis was done using the GPS-LS linker scanning system (New England Biolabs, Inc.) and the Mutation Generation System kit (Finnzymes). pENTR-*hZW10* served as the template for mutagenesis. *hZW10* point mutations were generated using the QuikChange site-directed mutagenesis kit (Stratagene) using pENTR-*hZW10* as the template. Exact sites of insertion as well as confirmation of point mutation were determined by sequencing using BigDye Terminators v3.1 (Applied Biosystems) and the ABI PRISM 310 capillary sequencer (Applied Biosystems).

Cell culture

HeLa and HEK293 cells were grown in DME with 10% FCS at 37°C in 5% CO₂. For FRAP experiments, HeLa cell media was supplemented with 1 M Hepes buffer (Invitrogen), pH 7.4, to a final concentration of 7 mM. Vinblastine was used at a final concentration of 0.1 μM unless otherwise stated. STLC was used at a final concentration of 7 μM.

Western blotting

HEK293 cells were grown to ~75% confluence and transfected for 24 h with 2 μg of plasmid DNA using 10 μl polyethyleneimine (PEI; 1 mg/ml; Cedarlane Laboratories Ltd.) diluted in 250 μl opti-MEM (Invitrogen). The cells were harvested for Western blotting as previously described (Chan et al., 1998). Western blotting was analyzed using mouse monoclonal anti-GFP antibodies conjugated to the IR800 dye (Rockland Immunochemicals, Inc.) at a 1:10,000 dilution or rabbit polyclonal anti-GST antibodies (Chan et al., 2000) at a 1:1,000 dilution detected with anti-rabbit polyclonal secondary antibodies conjugated to the Alexa Fluor 680 dye (Invitrogen) at a 1:10,000 dilution. *hZW10* was probed for using rabbit polyclonal antibodies against *hZW10* at a dilution of 1:1,000 (Chan et al., 2000) and detected using anti-rabbit Alexa Fluor 680 dye-conjugated secondary antibodies (Invitrogen) at a dilution of 1:10,000. Tubulin was probed for using the mouse monoclonal anti-tubulin antibody (B512; Sigma-Aldrich) at a dilution of 1:5,000 and detected using anti-mouse secondary antibodies conjugated to the IR800 dye at a dilution of 1:10,000. The blots were analyzed using the Odyssey scanner (LI-COR Biosciences) controlled by the Odyssey software (LI-COR Biosciences). Images were processed using Photoshop 7.0 (Adobe).

Fluorescence microscopy

HeLa cells grown on coverslips and transiently transfected with EGFP constructs or siRNA were processed for fluorescence microscopy as previously described (Chan et al., 2000; Liu et al., 2003). *hZW10* was visualized using rabbit anti-*hZW10* antibodies at a 1:1,500 dilution (Chan et al., 2000) and anticentromere antibody (ACA) was visualized using human ACA sera at a 1:3,000 dilution (gift from M. Fritzler, University of Calgary, Calgary, Canada). A microscope (AxioPlan2; Carl Zeiss, Inc.) equipped with epifluorescence optics was used to collect the images. Cells were visualized with a 100× Plan-Apochromatic objective with a (1.4 NA) and images were captured with a charge-coupled device camera (Photometrics CoolSNAP HQ; Roper Scientific), which was controlled with a personal computer running Metamorph software (v7.1; MDS Analytical Technologies). The coverslips were mounted using mowiol mounting media (EMD) and imaging was performed at room temperature. Image processing was performed using Photoshop 7.0.

Transient transfection and permanent cell line selection

HeLa cells grown to 60% confluence on coverslips in 35-mm dishes were transiently transfected with 2 μg of the EGFP constructs with 10 μl PEI (1 mg/ml) for 24 h. HEK293 cells were grown to 80% confluence in 35-mm dishes and transfected as the HeLa cells. For permanent cell line selection, HeLa cells were grown to ~80% confluence on 10-cm dishes that were cotransfected with 10 μg Xmn1-linearized EGFP-*hZW10* constructs and 10 μg BamH1-linearized pDNA3 vectors using 30 μl PEI (1 mg/ml) diluted in 1 ml opti-MEM for 48 h. After 48 h, G418 (Invitrogen) was added to a final concentration of 50 μg/ml and the cells were grown for ~2 wk. The surviving colonies were collected and cell sorted for GFP expression using a cell sorter (EPICS Altra HyPer; Beckman Coulter). The sorted cells were allowed to proliferate for ~1 wk and again sorted for GFP-expressing cells.

Kinetochoore localization of the EGFP-hZW10 constructs was confirmed using fluorescence microscopy.

Live cell FRAP

HeLa cells stably expressing EGFP-hZW10 or EGFP-hZW10^{N1} were plated onto 35-mm glass coverslip bottom dishes (FluoroDish; World Precision Instruments, Inc.). Experiments were performed using a multiphoton confocal scanning microscope (NLO 510; Carl Zeiss, Inc.) using a 63× Plan-apochromatic lens (1.4 NA) equipped with an objective and a stage warmer. FRAP was performed as previously described (Howell et al., 2004). Single kinetochores were laser ablated with 10 laser pulses and the subsequent fluorescence recovery was observed for 90–120 s at 1–10-s intervals. Data were collected using the LSM software (Carl Zeiss, Inc.), processed using Excel (Microsoft), and graphed using Prism software (GraphPad software). The recovered fluorescence intensity signal was calculated based on the area that was laser bleached. It was then normalized by subtraction of the background signal obtained from an area outside the cell that had the exact same dimensions as the ablated area. The recovered fluorescence intensity was then adjusted for photobleaching at each time point by measuring the decrease in total fluorescence of the entire cell. Once adjusted for background and photobleaching, the percentage of recovery of the fluorescence signal was calculated and graphed (nonlinear regression curve) versus time (Prism software). T_{1/2} values were extrapolated from the graphs and statistical analysis was done in Excel.

Yeast two hybrid

Yeast two-hybrid analysis was performed as previously described (Chan et al., 1998). The β-galactosidase assay was performed using the yeast β-galactosidase assay kit (Thermo Fisher Scientific) according to the manufacturer's protocol for quantitative analysis. Each assay was done in triplicate. Vectors and yeast strains were provided by E. Golemis (Fox Chase Cancer Center, Philadelphia, PA).

siRNA

hZW10 siRNA knockdown was achieved using Stealth siRNA (Invitrogen) that was designed after the previously described target sequence (Kops et al., 2005). HeLa cells were initially transfected with 100, 50, 25, or 12.5-nM final concentration siRNA using Oligofectamine (Invitrogen) according to the manufacturer's protocol and were analyzed 72 h after transfection. The 50-nM siRNA concentration, which had ~90% knockdown, was chosen for all remaining siRNA experiments.

GST pulldown

HEK293 cells were cotransfected with GST and EGFP constructs for 24 h. 10% of the cell lysate was immunoblotted for quantitation of the EGFP constructs using the Odyssey software. Normalized amounts of each cell lysate were incubated with glutathione Sepharose beads (GE Healthcare) for 3 h at 4°C. 10% of each normalized lysate was removed before addition of the beads as an input control. The beads were subsequently washed five times with 1% NP-40 lysis buffer (1% NP-40, 150 mM NaCl, 50 mM Tris-HCl, pH 8.0, supplemented with sodium pyrophosphate, sodium orthovanadate, NaF, β-glycerophosphate, DTT, leupeptin, aprotinin, chymostatin, AEBSF, and pepstatin), resuspended in 1× SDS-PAGE loading buffer and immunoblotted along with the input controls.

Online supplemental material

Fig. S1 outlines kinetochore localization analysis of the C- and N-terminal hZW10 truncation mutants. Fig. S2 outlines mapping of the hZW10 N-terminal hZwint-1 interaction domain through yeast two hybrid and GST pulldown. Fig. S3 outlines kinetochore localization analysis of the hZW10 5-aa insertion mutant library. Fig. S4 outlines the kinetochore localization analysis of the hZW10^{N1} 5-aa insertion mutant library and EGFP-hZW10^{N1} kinetochore dynamics in STLC-arrested cells. Fig. S5 outlines kinetochore localization analysis and the conservation of single amino acid substitution mutants within hZW10. Online supplemental material is available at <http://www.jcb.org/cgi/content/full/jcb.200708021/DC1>.

We would like to thank the members of the Chan laboratory for their encouragement and, particularly, Dr. Dawn Macdonald for editing and helpful discussion. We also thank Drs. Shelaugh Campbell, Martin Srayko, and Tim Yen for reading the manuscript and providing helpful suggestions. We acknowledge the generous gift of ACA antibodies from Dr. Marvin Fritzler. We thank Dr. Erica Golemis for providing the Lex-A-based yeast two-hybrid system. All microscopy experiments were performed at the Cross Cancer Institute Cell Imaging Facility.

J.K. Famulski is funded by a Canadian Graduate Scholarship Award from the Canadian Institute of Health Research and a Graduate Studentship from the

Alberta Cancer Board. L.J. Vos is funded by the 75th Anniversary Graduate Student Award from the Department of Medicine and Dentistry at the University of Alberta and the Postgraduate Scholarship-A from the National Science and Engineering Research Council. G.K. Chan is funded by the Canadian Institute of Health Research New Investigator Award (MSH69137). This research is funded by grants from the Canadian Institute of Health Research (MOP57723), the Alberta Cancer Board (21594), the Canadian Foundation for Innovation (G125000560, project number 9569), the Alberta Heritage Foundation for Medical Research (200301326 and 200201828), and the Alberta Science and Research Authority (G230000164).

Submitted: 3 August 2007

Accepted: 8 January 2008

References

- Basto, R., R. Gomes, and R.E. Karess. 2000. Rough deal and Zw10 are required for the metaphase checkpoint in *Drosophila*. *Nat. Cell Biol.* 2:939–943.
- Basto, R., F. Scaerou, S. Mische, E. Wojcik, C. Lefebvre, R. Gomes, T. Hays, and R. Karess. 2004. In vivo dynamics of the rough deal checkpoint protein during *Drosophila* mitosis. *Curr. Biol.* 14:56–61.
- Buffin, E., C. Lefebvre, J. Huang, M.E. Gagou, and R.E. Karess. 2005. Recruitment of Mad2 to the kinetochore requires the Rod/Zw10 complex. *Curr. Biol.* 15:856–861.
- Chan, G.K., B.T. Schaar, and T.J. Yen. 1998. Characterization of the kinetochore binding domain of CENP-E reveals interactions with the kinetochore proteins CENP-F and hBUBR1. *J. Cell Biol.* 143:49–63.
- Chan, G.K., S.A. Jablonski, D.A. Starr, M.L. Goldberg, and T.J. Yen. 2000. Human Zw10 and ROD are mitotic checkpoint proteins that bind to kinetochores. *Nat. Cell Biol.* 2:944–947.
- Chan, G.K., S.T. Liu, and T.J. Yen. 2005. Kinetochore structure and function. *Trends Cell Biol.* 15:589–598.
- Cheeseman, I.M., S. Niessen, S. Anderson, F. Hyndman, J.R. Yates III, K. Oegema, and A. Desai. 2004. A conserved protein network controls assembly of the outer kinetochore and its ability to sustain tension. *Genes Dev.* 18:2255–2268.
- Hori, T., T. Haraguchi, Y. Hiraoka, H. Kimura, and T. Fukagawa. 2003. Dynamic behavior of Nuf2-Hec1 complex that localizes to the centrosome and centromere and is essential for mitotic progression in vertebrate cells. *J. Cell Sci.* 116:3347–3362.
- Howell, B.J., B.F. McEwen, J.C. Canman, D.B. Hoffman, E.M. Farrar, C.L. Rieder, and E.D. Salmon. 2001. Cytoplasmic dynein/dynactin drives kinetochore protein transport to the spindle poles and has a role in mitotic spindle checkpoint inactivation. *J. Cell Biol.* 155:1159–1172.
- Howell, B.J., B. Moree, E.M. Farrar, S. Stewart, G. Fang, and E.D. Salmon. 2004. Spindle checkpoint protein dynamics at kinetochores in living cells. *Curr. Biol.* 14:953–964.
- Jordan, M.A., D. Thrower, and L. Wilson. 1992. Effects of vinblastine, podophyllotoxin and nocodazole on mitotic spindles. Implications for the role of microtubule dynamics in mitosis. *J. Cell Sci.* 102:401–416.
- Karess, R. 2005. Rod-Zw10-Zwilch: a key player in the spindle checkpoint. *Trends Cell Biol.* 15:386–392.
- Karess, R.E., and D.M. Glover. 1989. *rough deal*: a gene required for proper mitotic segregation in *Drosophila*. *J. Cell Biol.* 109:2951–2961.
- Kops, G.J., Y. Kim, B.A. Weaver, Y. Mao, I. McLeod, J.R. Yates III, M. Tagaya, and D.W. Cleveland. 2005. ZW10 links mitotic checkpoint signaling to the structural kinetochore. *J. Cell Biol.* 169:49–60.
- Lin, Y.T., Y. Chen, G. Wu, and W.H. Lee. 2006. Hec1 sequentially recruits Zwint-1 and ZW10 to kinetochores for faithful chromosome segregation and spindle checkpoint control. *Oncogene.* 25:6901–6914.
- Liu, S.T., G.K. Chan, J.C. Hittle, G. Fujii, E. Lees, and T.J. Yen. 2003. Human MPS1 kinase is required for mitotic arrest induced by the loss of CENP-E from kinetochores. *Mol. Biol. Cell.* 14:1638–1651.
- Musacchio, A., and E.D. Salmon. 2007. The spindle-assembly checkpoint in space and time. *Nat. Rev. Mol. Cell Biol.* 8:379–393.
- Obuse, C., O. Iwasaki, T. Kiyomitsu, G. Goshima, Y. Toyoda, and M. Yanagida. 2004. A conserved Mis12 centromere complex is linked to heterochromatic HP1 and outer kinetochore protein Zwint-1. *Nat. Cell Biol.* 6:1135–1141.
- Rieder, C.L., A. Schultz, R. Cole, and G. Sluder. 1994. Anaphase onset in vertebrate somatic cells is controlled by a checkpoint that monitors sister kinetochore attachment to the spindle. *J. Cell Biol.* 127:1301–1310.
- Scaerou, F., I. Aguilera, R. Saunders, N. Kane, L. Blottiere, and R. Karess. 1999. The rough deal protein is a new kinetochore component required for accurate chromosome segregation in *Drosophila*. *J. Cell Sci.* 112:3757–3768.

- Scaerou, F., D.A. Starr, F. Piano, O. Papoulas, R.E. Karess, and M.L. Goldberg. 2001. The ZW10 and Rough Deal checkpoint proteins function together in a large, evolutionarily conserved complex targeted to the kinetochore. *J. Cell Sci.* 114:3103–3114.
- Shah, J.V., E. Botvinick, Z. Bondy, F. Furnari, M. Berns, and D.W. Cleveland. 2004. Dynamics of centromere and kinetochore proteins; implications for checkpoint signaling and silencing. *Curr. Biol.* 14:942–952.
- Skibbens, R.V., C.L. Rieder, and E.D. Salmon. 1995. Kinetochore motility after severing between sister centromeres using laser microsurgery: evidence that kinetochore directional instability and position is regulated by tension. *J. Cell Sci.* 108:2537–2548.
- Skoufias, D.A., S. DeBonis, Y. Saoudi, L. Lebeau, I. Crevel, R. Cross, R.H. Wade, D. Hackney, and F. Kozlinski. 2006. S-trityl-L-cysteine is a reversible, tight binding inhibitor of the human kinesin Eg5 that specifically blocks mitotic progression. *J. Biol. Chem.* 281:17559–17569.
- Starr, D.A., B.C. Williams, Z. Li, B. Etemad-Moghadam, R.K. Dawe, and M.L. Goldberg. 1997. Conservation of the centromere/kinetochore protein ZW10. *J. Cell Biol.* 138:1289–1301.
- Starr, D.A., B.C. Williams, T.S. Hays, and M.L. Goldberg. 1998. ZW10 helps recruit dynein and dynein to the kinetochore. *J. Cell Biol.* 142:763–774.
- Starr, D.A., R. Saffery, Z. Li, A.E. Simpson, K.H. Choo, T.J. Yen, and M.L. Goldberg. 2000. HZWint-1, a novel human kinetochore component that interacts with HZW10. *J. Cell Sci.* 113:1939–1950.
- Sudakin, V., G.K. Chan, and T.J. Yen. 2001. Checkpoint inhibition of the APC/C in HeLa cells is mediated by a complex of BUBR1, BUB3, CDC20, and MAD2. *J. Cell Biol.* 154:925–936.
- Toby, G.G., and E.A. Golemis. 2001. Using the yeast interaction trap and other two-hybrid-based approaches to study protein-protein interactions. *Methods.* 24:201–217.
- Wang, H., X. Hu, X. Ding, Z. Dou, Z. Yang, A.W. Shaw, M. Teng, D.W. Cleveland, M.L. Goldberg, L. Niu, and X. Yao. 2004. Human Zwint-1 specifies localization of Zeste White 10 to kinetochores and is essential for mitotic checkpoint signaling. *J. Biol. Chem.* 279:54590–54598.
- Wang, Z., J.M. Cummins, D. Shen, D.P. Cahill, P.V. Jallepalli, T.L. Wang, D.W. Parsons, G. Traverso, M. Awad, N. Silliman, et al. 2004. Three classes of genes mutated in colorectal cancers with chromosomal instability. *Cancer Res.* 64:2998–3001.
- Williams, B.C., and M.L. Goldberg. 1994. Determinants of *Drosophila zw10* protein localization and function. *J. Cell Sci.* 107:785–798.
- Williams, B.C., T.L. Karr, J.M. Montgomery, and M.L. Goldberg. 1992. The *Drosophila l(1)zw10* gene product, required for accurate mitotic chromosome segregation, is redistributed at anaphase onset. *J. Cell Biol.* 118:759–773.
- Williams, B.C., M. Gatti, and M.L. Goldberg. 1996. Bipolar spindle attachments affect redistributions of ZW10, a *Drosophila* centromere/kinetochore component required for accurate chromosome segregation. *J. Cell Biol.* 134:1127–1140.
- Williams, B.C., Z. Li, S. Liu, E.V. Williams, G. Leung, T.J. Yen, and M.L. Goldberg. 2003. Zwilch, a new component of the ZW10/ROD complex required for kinetochore functions. *Mol. Biol. Cell.* 14:1379–1391.
- Wojcik, E., R. Basto, M. Serr, F. Scaerou, R. Karess, and T. Hays. 2001. Kinetochore dynein: its dynamics and role in the transport of the Rough deal checkpoint protein. *Nat. Cell Biol.* 3:1001–1007.
- Yang, Z., U.S. Tulu, P. Wadsworth, and C.L. Rieder. 2007. Kinetochore dynein is required for chromosome motion and congression independent of the spindle checkpoint. *Curr. Biol.* 17:973–980.